Dynamics of the one-dimensional Anderson insulator coupled to various bosonic baths

Janez Bonča,[1,2] Stuart A. Trugman,[3] and Marcin Mierzejewski[4]
[1]*Faculty of Mathematics and Physics, University of Ljubljana, SI-1000 Ljubljana, Slovenia*
[2]*Jožef Stefan Institute, SI-1000 Ljubljana, Slovenia*
[3]*Center for Integrated Nanotechnologies, Los Alamos National Laboratory, Los Alamos, New Mexico, USA*
[4]*Department of Theoretical Physics, Faculty of Fundamental Problems of Technology, Wrocław University of Science and Technology, 50-370 Wrocław, Poland*

(Received 30 December 2017; published 9 May 2018)

We study a particle which propagates in a one-dimensional strong random potential and is coupled to a bosonic bath. We independently test various properties of bosons (hopping term, hard-core effects, and generic boson-boson interaction) and show that bosonic itineracy is the essential ingredient governing the dynamics of the particle. Coupling of the particle to itinerant phonons or hard-core bosons alike leads to delocalization of the particle by virtue of a subdiffusive (or diffusive) spread from the initially localized state. Delocalization remains in effect even when the boson frequency and the bandwidth of itinerant bosons remain an order of magnitude smaller than the magnitude of the random potential. When the particle is coupled to localized bosons, its spread remains logarithmic or even sublogarithmic. The latter result together with the survival probability shows that the particle remains localized despite being coupled to bosons.

DOI: 10.1103/PhysRevB.97.174202

I. INTRODUCTION

The interplay between disorder and many-body interactions is a long-standing problem which is important for the presence of the Anderson localization (AL) [1] in realistic materials. While the problem was recognized many years ago [2,3], recently there has been significant progress in understanding the physics of the many-body localization (MBL) which extends the concept of AL by accounting for interactions between the localized particles [4,5]. The presence of MBL in strongly disordered chains of spinless fermions (or equivalent models) has consistently been confirmed by various theoretical investigations [6–23] and a few experimental studies [24–29]. The many-body interaction is responsible for several distinctive features of the MBL systems, in particular for the unusually slow dynamics [30–48].

The particle localization is not immune against arbitrary many-body interaction, and mechanisms which are known to destroy the Anderson insulator may destroy the MBL as well. In particular, the Anderson insulator may be destroyed by the electron-phonon interaction via the so-called phonon-assisted hopping [49,50]. However, the insulating state may still survive in the low-temperature regime, as recently suggested in Refs. [51,52]. The phonon-assisted hopping has been intensively studied and is mostly understood for regular noninteracting bosons [50]. However, already the case of strictly dispersionless phonons may pose problems, especially in one-dimensional (1D) systems [50]. The role of other bosonic excitations (e.g., magnons) or the boson-boson interaction remains unexplored. In particular, it is an open problem whether coupling between charge carriers and magnetic excitations [47,53–58] may play the same role as the electron-phonon coupling. The essential difference between both types of bosons is that the energy density of the magnetic excitations is bounded from above, whereas phonons can in principle absorb arbitrary energy.

Here, we study a single particle in a disordered chain which is coupled to bosons. We aim to establish which properties of the bosonic system are essential for preserving/destroying the localized state. In particular, we study systems with regular bosons (e.g., phonons) and hard-core (HC) bosons, whereby the latter case should simulate spin excitations. We compare results for itinerant and localized/dispersionless bosons as well as interacting and noninteracting bosons. We find that itineracy is essential for localization. We show that for sufficiently strong disorder the particle is localized despite coupling to localized hard-core bosons. However, even very small bosonic dispersion destroys localization and leads to a subdiffusive hole propagation, which may eventually turn into the diffusive transport at extremely long timescale. In the system of itinerant noninteracting bosons the particle and energy transport is ballistic. In order to eliminate artifacts originating from this peculiarity of the bosonic subsystem, we consider also a generic case with boson-boson interaction when the energy transport within the bosonic subsystem is diffusive. It turns out that the latter interaction hardly influences propagation of the coupled particle. Finally, the transport in the strongly disordered Holstein model with dispersionless regular bosons is shown to be indeed singular since the particle spreads out logarithmically or sublogarithmically in time.

II. MODEL AND METHOD

We investigate the Anderson localization in the one-dimensional model with a single electron in a random potential $\epsilon_j \in [-W, W]$ coupled to bosonic degrees of

freedom:

$$H = -t_0 \sum_j [c_j^\dagger c_{j+1} + \text{H.c.} + \epsilon_j n_j] - g \sum_j n_j (b_j^\dagger + b_j) + \omega \sum_j b_j^\dagger b_j + t_b \sum_j [b_j^\dagger b_{j+1} + \text{H.c.}] + V_1 \sum_j m_j m_{j+1} + V_2 \sum_j m_j m_{j+2}, \quad (1)$$

where $n_j = c_j^\dagger c_j$ represents the electron number operator, b_j represents either phonon or HC boson, and $m_j = b_j^\dagger b_j$ is the boson number operator. The strength of electron-boson interaction is given by g, and ω is the bosonic frequency. Dispersion of otherwise localized bosonic degrees of freedom is introduced via the overlap integral t_b, while V_1 and V_2 represent nearest and next-nearest neighbor bosonic interaction strengths. We separately consider standard bosons and the HC bosons. The former case is relevant for systems where the quantum particle (c_i) is coupled to optical phonons (b_i) with frequency ω. Then, $[b_i, b_j^\dagger] = \delta_{ij}$ and, in principle, the density of bosonic excitations may be arbitrarily large. Choosing $V_1 = V_2 = 0$ one obtains the standard Holstein model. The results for HC bosons simulate coupling to spin fluctuations. In this case, the energy spectrum is bounded from above since there is at most one HC boson per site, $b_i^\dagger b_i^\dagger = 0$. This restriction shows up in specific commutation relations $[b_i, b_j^\dagger] = \delta_{ij}(1 - 2b_i^\dagger b_i)$ for the latter operators. We perform calculations for one-dimensional chains of various length sizes with open boundary conditions. We perform time evolution using a Lanczos based technique and use the limited functional Hilbert space (LFHS) first developed in Ref. [59]. In the Appendix A we give a brief overview of the method. Such an approach has successfully been applied to studies on the real-time dynamics of t-J and Holstein models [47,60–67]. This method enabled calculations on larger chains with open boundary conditions where the maximal distance between the electron and boson excitation is given by N_h. When the numerical calculations are carried out for systems of size L, the finite-size analysis usually consists in fitting the results by a function which is linear in $1/L$. In the present approach, we find the best fits which are linear in $1/N_h$ and then we take the limit $N_h \to \infty$ for the fitting function.

III. NUMERICAL RESULTS

We start the time evolution from a random configuration of bosonic degrees of freedom and a well defined original position of the coupled particle. We typically take 1400 realizations of the disorder. In the case of the HC boson (HCB) such a choice of the initial state represents propagation at infinite temperature. This is not the case for the Holstein model due to the unlimited number of phonon degrees of freedom. In the latter case the temperature of the bosonic subsystem is quite elevated but still finite. In the Appendix B we discuss how results depend on the initial state of the bosonic bath. We measure time in units of $[\hbar/t_0]$; in addition for simplicity we set in all cases $t_0 = \omega = g = 1$.

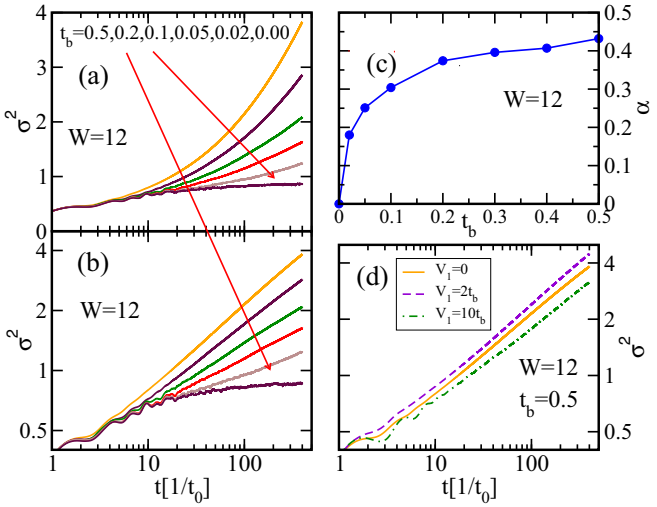

FIG. 1. The mean square deviation $\sigma^2(t)$ for different values of t_b for the case when the particle is coupled to HCBs using (a) semilog plot and (b) log-log plot; (c) fitting exponents α vs t_b extracted from $\sigma^2(t) = At^\alpha$. Fitting was performed in the long-time limit. (d) log-log plot of $\sigma^2(t)$ of the HCB model using different values of nearest and next nearest interaction V_1 and V_2, respectively. In all cases we have used $\omega = g = 1$, $W = 12$, and $N_h = 20$.

In order to investigate the dynamics of the charge carrier we calculate the particle density

$$\rho_j = \langle \psi(t) | n_j | \psi(t) \rangle_{\text{ave}}, \quad (2)$$

where the index "ave" signifies that expectation values have been averaged over different random realizations of ϵ_j. Since the density is normalized, $\sum_j \rho_j = 1$, we also define the mean square deviation of the hole distribution [68],

$$\sigma^2 = \sum_j j^2 \rho_j - \left[\sum_j j \rho_j \right]^2. \quad (3)$$

We start by presenting results for the HCB model. In Fig. 1 we present the time evolution of σ^2 at large disorder $W = 12$. In the case of localized HCBs, i.e., when $t_b = 0$, $\sigma^2(t)$ approaches a constant, indicating particle localization. In contrast, even a small value of dispersion $t_b > 0$ already leads to a power-law behavior, i.e., $\sigma^2 \propto t^\alpha$, clearly demonstrated as a straight line on the log-log plot; see Fig. 1(b). It is also instructive to note that the timescale when the power law sets in is roughly given by $1/t_b$, most clearly observed as a deviation from the straight line in Fig. 1(b). In Fig. 1(c) we display extracted exponents $\alpha(t_b)$. They appear to be nonuniversal and characteristic of a subdiffusive spread of the initially localized particle. Moreover, in the whole range of t_b their values remain $\alpha(t_b) < 0.5$, which is far below $\alpha = 1$ that is distinctive for the diffusive spread. From our analysis we may extrapolate that $\alpha(t_b > 0) > 0$, suggesting that the particle remains localized only in the dispersionless limit when HCBs are strictly localized, i.e., at $t_b = 0$. This is perhaps expected from the point of view of variable range hopping theory [69] and Fermi golden rule, which assumes that the bosons created in the inelastic hopping process spread out to infinity, hence the probability for the reabsorption by the electron drops to zero.

Nonzero t_b lets bosons spread out. In contrast, at zero t_b they remain in the vicinity of the particle, consequently an emitted boson can be reabsorbed to reverse the hopping process.

So far we have shown that already a small amount of dispersion among HCBs leads to a delocalization of a particle in a one-dimensional random potential. This holds true even when the magnitude of the random potential W by far exceeds the boson frequency ω and the bandwidth $\Gamma = 4t_b$. Next we investigate the influence of interactions between HCBs. In Fig. 1(d) we present results for a fixed value of disorder, at finite value of t_b but different choices of nearest and next-nearest interactions, V_1 and V_2, respectively. We further fix the value of $V_2 = V_1/2$. The reason for the choice of a finite value of V_2 is that at $V_2 = 0$ the system of interacting HCBs with zero coupling to the particle is exactly solvable and shows ballistic energy transport. One expects that the electron-phonon coupling alone is sufficient to restore the normal diffusive transport in the bosonic subsystem, even for $V_1 = V_2 = 0$. It is clearly the case for nonzero concentration of particles. However, this mechanism may not be efficient for the present case of a single particle which couples to a much larger bosonic bath since the relevant timescale for the onset of normal transport may be very long. In comparison to the $V_1 = 0$ case, we observe a slight increase of $\sigma^2(t)$ at small $V_1 = 2t_b$ followed by a decrease with further increasing of V_1 towards $V_1 = 10t_b$. In the latter case we also observe a small decrease of α. Interactions among HCBs have only a small effect on the delocalization processes. The slight increase in $\sigma^2(t)$ at small values of V_1 can be due to lifting of the degeneracy among many-body HCB states in the presence of interactions. However, further increase of V_1 may lead to slowing down of the propagation of excitations in the HCB subspace that seem to be responsible for the delocalization of the particle.

We have tested the validity of our findings with regard to finite-size effects as well as regarding the effect of limited functional Hilbert spaces used in our calculations. The size of the LFHS exponentially depends on the parameter N_h. For a more precise explanation of the meaning of N_h, we refer the reader to Appendix A as well as to the original publication in Ref. [59]. Here we only note that N_h represents the maximal length that the particle travels from its original position, while the maximal number of HCBs is given by $N_h/2$. In Fig. 2 we show results for two different values of disorder, obtained with different Hilbert spaces. When HCBs are localized, i.e., for $t_b = 0$, the particle also remains localized, see Figs. 2(a) and 2(c), even after the finite-size analysis. In particular, at $W = 8$ we observe a logarithmic increase of $\sigma^2(t)$, characteristic for MBL systems [42,70], while at yet stronger disorder, $W = 12$, we observe a tendency towards the saturation similar to the case of a noninteracting particle (see curve for $g = 0$). However, in contrast to the noninteracting system, strict saturation does not arise within the accessible time window, and the extremely slow dynamics resembles the MBL systems rather than noninteracting AL.

In contrast, in the case of itinerant HCBs, that is at finite dispersion $t_b = 0.5$, we observe subdiffusion; see Figs. 2(b) and 2(d). Dashed lines in all cases represent results obtained using finite-size scaling analysis. For finite dispersion, we have obtained nearly perfect fits, presented with dotted lines, to the analytical form $\sigma^2(t) = At^\alpha$. We have performed a similar analysis as well for smaller values of $W = 6$ and 4, not shown. In the inset of Fig. 2(b) we show extracted α's that are increasing towards $\alpha = 1$ as the disorder decreases. Due to increasing finite-size effects we were unable to reliably investigate systems with $W < 4$.

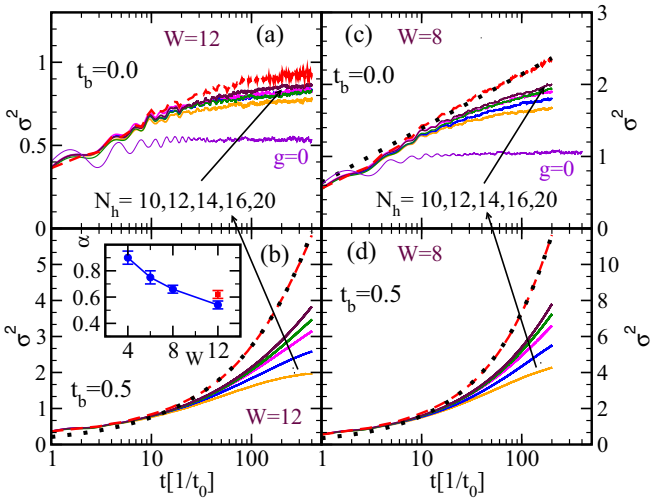

FIG. 2. Semilog plots of $\sigma^2(t)$ of the HCB model for different sizes of the Hilbert spaces generated by N_h. Cases with no dispersion, $t_b = 0$, are presented in (a) and (c) for two distinct values of disorder $W = 12$ and 8, respectively. Results for $t_b = 0.5$ are shown as well for two distinct values of W in (b) and (d). Note also substantially different scales used to present results with or without dispersion. Dashed (red) lines represent results after finite-size scaling analysis. The dotted line in (c) represents a fit to the form $\sigma^2(t) = A + B\log(t)$. Dotted lines in (b) and (d) represent fits to the form $\sigma^2(t) = At^\alpha$. The thin (violet in color) line in (a) and (c) represents evolution of $\sigma^2(t)$ for a free particle, i.e., $g = 0$, that is subject to Anderson's localization. The inset in (b) displays exponents α (circles) extracted from finite-size scaled results at different values of disorder W. A singular square represents the result for the Holstein model with parameters identical to those in the HCB one. Other parameters of the model were $\omega = g = 1$ and $V_1 = V_2 = 0$.

We next present results for the Holstein model. Due to unlimited phonon degrees of freedom we had to limit our calculations to a maximal number of phonons, given by N_h. Similarly to the HCB model case, N_h represents also the maximal distance that the particle travels from the origin, while $N_h - 1$ is the maximal distance between the particle and a single phonon excitation. We start the time evolution from an initial random configuration of phonon degrees of freedom and well defined initial position of the particle. We present results in Fig. 3 for a single set of parameters, i.e., $W = 12$ as well as at fixed $g = 1$. The discussion of the influence of increasing coupling constant from weak towards strong coupling limit for the Holstein model is presented in Appendix C. In the case of localized phonons, i.e., $t_b = 0$, we observe slow, logarithmic increase of $\sigma^2(t)$; see Fig. 3(a). Since we have used parameters identical to those in the HCB model, Figs. 2(a) and 3(a) provide direct comparison between the models. While in the case of the HCB model $\sigma^2(t)$ shows signs of saturation or at most sublogarithmic growth, we observe a clear logarithmic growth when the particle is coupled to

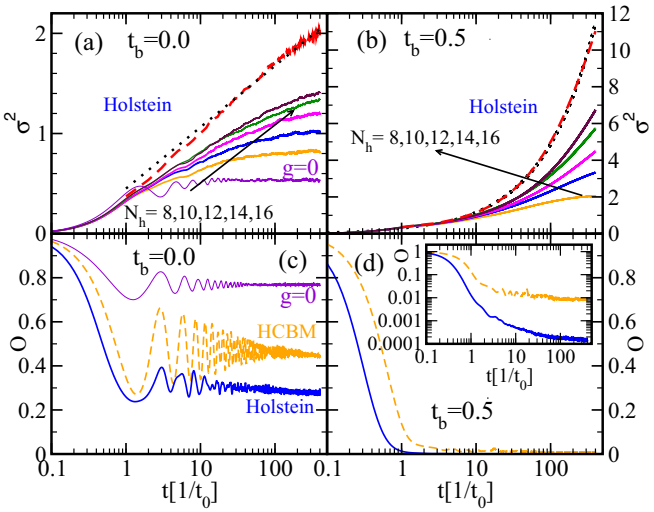

FIG. 3. (a) and (b) $\sigma^2(t)$ of the Holstein model for different sizes of the Hilbert spaces generated by N_h and $W = 12$. The cases with no dispersion, $t_b = 0$, are presented in (a) while results for $t_b = 0.5$ are shown (b). Dashed (red) lines represent results after finite-size scaling analysis. The dotted line in (a) represents a fit to the form $\sigma^2(t) = A + B\log(t)$. The dotted line in (b) represents a fit to the form $\sigma^2(t) = At^\alpha$. Overlaps $\mathcal{O}$ are shown in (c) ($t_b = 0$) and (d) ($t_b = 0.5$) for the Holstein model with full lines and for the HCB model with dashed lines. Thin lines (violet in color) in (a) and (c) represent evolution of $\sigma^2(t)$ and $\mathcal{O}$, respectively, for a free particle, i.e., at $g = 0$, that undergoes Anderson's localization. The inset in (d) shows the same data as in (d) but using log-log scale. Other parameters of the model were in all cases $\omega = g = 1$, $W = 12$, and $V_1 = V_2 = 0$.

regular bosons (phonons). Moreover, its spread is enhanced in comparison to the HCB case and displays quantitatively distinct behavior from the noninterracting case at $g = 0$. A similar comparison is found as well in the case of finite dispersion. Coupling to itinerant phonons again leads to a subdiffusive growth of $\sigma^2(t)$, see Fig. 3(b), with an exponent $\alpha = 0.62$ that is about 10% larger than in the case of the HCB model; for visual comparison see also the inset of Fig. 2(b). However, one cannot exclude that in this model there exists a small, albeit nonzero diffusion constant. Then, the subdiffusion would be a transient effect since the spread due to normal diffusion will dominate at sufficiently long time. Suppression of transport in the case when particle is coupled to marginally localized phonons has recently been demonstrated in Ref. [71] for the low-temperature regime.

Finally, we investigate the survival probability defined as the overlap of the many-body wave function $|\psi(t)\rangle$ with the initial one $|\psi(0)\rangle$ [15,72,73]. Namely, we compute

$$\mathcal{O}(t) = |\langle\psi(0)|\exp(-iHt)|\psi(0)\rangle|^2_{\text{ave}}. \tag{4}$$

It measures the probability of finding the system still in the initial state $|\psi(0)\rangle$ at time t [15]. In the case of localized bosons, $t_b = 0$ presented in Fig. 3(c), $\mathcal{O}(t)$ approaches a constant in the long-time limit. In addition, well defined oscillations with a frequency $\omega \sim 2$ are observed at moderate times that are more pronounced in the HCB model case. They signal transitions among only a few states. The specific value of the frequency originates from the disorder averaging, and indicates that the charge dynamics is well restricted to the neighboring sites [43]. In contrast, in the case of itinerant bosons, Fig. 3(d), $\mathcal{O}(t \to \infty) \to 0$ while oscillations are strongly overdamped. The survival probability turned out to be very useful in the studies concerning the many-body localization [15,73], where $\mathcal{O}(t)$ decays exponentially with the system size L [73], $\mathcal{O}(t \gg 1) \sim \exp(-aL)$. The latter holds true in the MBL as well as in the ergodic regimes, whereby the parameter a in the localized system is much smaller than in the ergodic case. In the present studies, we have found a clear exponential decay with N_h (a quantity equivalent to L) only for systems with itinerant bosons; see the discussion in Appendix D. In contrast, in systems with localized bosons the dependence of $\mathcal{O}(t \gg 1)$ on the system size is rather small. The survival probability is constructed in terms of the many-body wave function of the total system. Then, the finite value of $\mathcal{O}(t)$ in the long-time limit and weak N_h dependence indicate not only localization of the particle but also freezing of the initial distribution of bosons with $t_b = 0$.

IV. CONCLUSIONS

We have studied the time evolution of a particle in a strong random potential coupled to localized or itinerant bosonic degrees of freedom. The study was based on a Holstein-like model in one dimension. Two types of bosons, i.e., hard-core bosons and phonons, were used in our study. The main motivation to study hard-core bosons was on the one hand their similarity to spin degrees of freedom and on the other their limited degrees of freedom that allowed studying larger system sizes. The coupling of the particle to itinerant bosons, HCBs and phonons alike, leads to delocalization by virtue of a subdiffusive spread from the initially localized state. Even more surprisingly, delocalization remains in effect even when the boson frequency and the bandwidth of itinerant bosons remain an order of magnitude smaller than the magnitude of the random potential. From among all the discussed properties of the bosonic bath, the itineracy of bosons plays the crucial role for the dynamics of the interacting particle.

We expect for dispersive standard bosons that the subdiffusive transport may be a long-lasting but still a transient phenomenon. On a very long timescale, the particle dynamics should be similar to that discussed in Ref. [19] where, instead of phonons, the quantum particle is coupled to a classical noise. However for strongly disordered systems, the timescale corresponding to the onset of standard diffusion is beyond the reach of direct numerical calculations for many-body quantum systems. An even more challenging question concerns the asymptotic dynamics of a particle coupled to the hard-core bosons.

ACKNOWLEDGMENTS

J.B. acknowledges financial support from the Slovenian Research Agency (research core funding No. P1-0044) and M.M. acknowledges support by the project 2016/23/B/ST3/00647 of the National Science Centre, Poland. S.A.T. acknowledges support from CINT. This work was performed, in part, at the Center for Integrated Nanotechnologies, a U.S. Department of Energy, Office of Basic Energy Sciences user facility.

APPENDIX A: GENERATOR OF LIMITED FUNCTIONAL HILBERT SPACE

We only give a short description of the main parts of the method. More details can be found in the original work, Ref. [59]. We choose the generator of the limited functional Hilbert space (LFHS) that consists of two off-diagonal parts of the Hamiltonian in Eq. (1) of the main text,

$$\mathcal{O}_1 = \sum_j n_j (b_j^\dagger + b_j), \tag{A1}$$

$$\mathcal{O}_2 = \sum_j c_j^\dagger c_{j+1} + \text{H.c.} \tag{A2}$$

The generating algorithm starts from a particle at a given position, e.g., $j = 0$, in a vacuum state of boson excitations, $|\psi^{(0)}\rangle = c_{0\sigma}^\dagger |0\rangle$, where $|0\rangle$ represents vacuum for the particle as well as boson excitations. We then apply the generator of basis states N_h times to generate the LFHS:

$$\{|\psi^{(l)}\rangle\} = (\mathcal{O}_1 + \mathcal{O}_2)^l |\psi_{(0)}\rangle, \tag{A3}$$

for $l = 0, \ldots, N_h$. We thus generate a limited functional Hilbert space spanned by states of the following form:

$$|\psi\rangle = |j; \ldots, n_{j-1}, n_j, n_{j+1}, \ldots\rangle \tag{A4}$$

where j represents the particle coordinate, while there are n_m bosons on site m. In the HCB case, $n_j \in \{0,1\}$ while for phonons $n_j \in \{0, \ldots, N_h\}$. The limited functional Hilbert space that we construct is not a standard one where bosonic degrees of freedom would be distributed uniformly on the lattice irrespective to the particle position. Our approach adds basis states more efficiently than some other methods. In the case of generating phonon degrees of freedom, a basis state is included if it can be reached using N_b phonon creation operators and N_t particle hops in any order with $N_b + N_t \leqslant N_h$. For a given N_h, there is a basis state with N_h phonon quanta on the same site as the particle and no phonon excitations elsewhere. The particle can hop maximally N_h sites away from its original position, but then there is no boson nor phonon quanta in the system. In the HCB case the maximal number of boson quanta is $N_h/2$. It is achieved by successive process where a HCB is created on site j followed by a jump to site $j+1$. In the case of LFHS we impose open boundary conditions. After completing generation of LFHS we time evolve the wave function using the Hamiltonian in Eq. (1) of the main text while taking advantage of the standard Lanczos-based diagonalization technique. Sizes of LFHS for the HCB model span from $N_{\text{st}} \sim 10^3$ for $N_h = 10$ up to 2×10^5 for the largest $N_h = 20$ used in our calculations. Sizes of LFHS for the Holstein model span from $N_{\text{st}} \sim 10^3$ for $N_h = 8$ up to 5×10^5 for the largest $N_h = 16$. To achieve sufficient accuracy of time propagation, we have used time-step size $\Delta t = 0.02$ and performed up to 2×10^4 time steps. In addition we have sampled over 10^3 different realizations of disorder ϵ_i.

The main advantage of LFHS over the exact diagonalization approach is to significantly reduce the dimension of the Hilbert space. The method has been successful in computing properties of the driven Holstein polaron [65], dissociation of a driven bipolaron [74], relaxation dynamics and thermalization properties of a highly excited polaron [64,66,67], as well as static and dynamic properties [63] and nonequilibrium dynamics [60–62] of correlated electron systems.

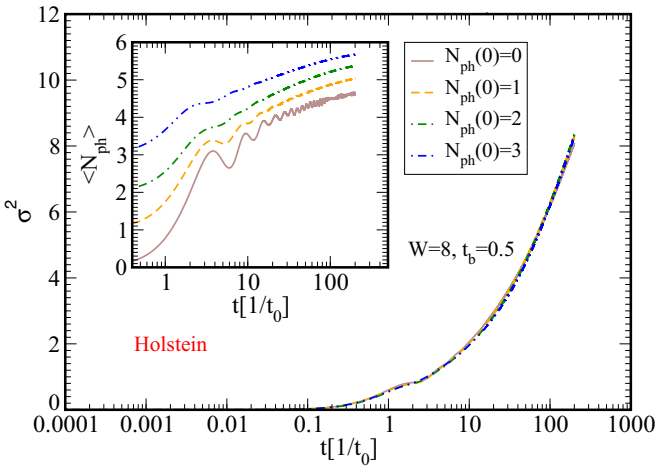

FIG. 4. σ^2 vs t for the Holstein model. $N_{\text{ph}}(0)$ the number of phonon excitations at $t = 0$. The inset represents $\langle N_{\text{ph}}\rangle(t)$. In both cases we have used $\omega = g = 1$, $t_b = 0.5$, and $W = 8$.

APPENDIX B: INITIAL STATE OF THE BOSONIC BATH

We test the dependence of σ^2 on the initial state of the bosonic bath in the case of the Holstein model. In Fig. 4 we present $\sigma^2(t)$ obtained by starting the time propagation from random initial states characterized by different total numbers of bosonic excitations $\langle N_{\text{ph}}\rangle \in \{0,1,2,3\}$, where $N_{\text{ph}} = \sum_j b_j^\dagger b_j$. In the inset of Fig. 4 we also follow the time evolution of $\langle N_{\text{ph}}\rangle(t)$. Different initial states in the long-time limit evolve towards distinct bosonic states; nevertheless, the spread of the initially localized particle $\sigma^2(t)$ remains nearly independent of the state of the bosonic subspace.

In the case of thermal equilibrium, different values of $\langle N_{\text{ph}}\rangle$ correspond to different temperatures. It should be noted, however, that the system under consideration is initially not in the thermal state. Figure 1(d) in the main text shows that the spread of the quantum particle in the HCB model is weakly modified by the boson-boson interaction even for very strong potentials V_1 and V_2. Since the latter interaction should lead to a rather fast thermalization of the bosonic bath, we come to conclusion that the nonthermal initial state of the bosonic bath does not influence the spread of the particle, at least not on a qualitative level.

APPENDIX C: STRONG COUPLING LIMIT

Here we explore the influence of the coupling constant g on the dynamics of the particle. We first introduce the dimensionless coupling constant $\lambda = g^2/2\omega t_0$. It is well known that $\lambda \sim 1$ represents the transition point between the weak-coupling regime for $\lambda \lesssim 1$ and the strong coupling one for $\lambda \gtrsim 1$. In the latter the polaron effective mass scales approximately as $m^* \propto \exp(g^2)$. The naive expectation is then that by increasing λ the particle would become nearly localized due to the exponentially increased m^*. In contrast, as shown in Fig. 5, the increase of λ leads to a monotonic increase of σ^2. It should

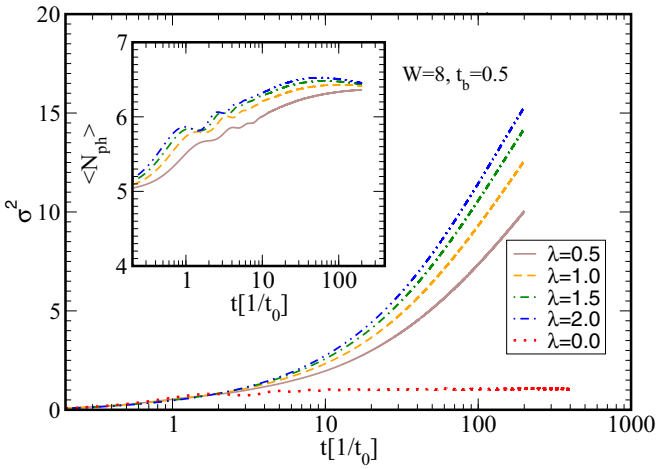

FIG. 5. σ^2 vs t for the Holstein model for different coupling strengths λ. The inset represents $\langle N_{\rm ph}\rangle(t)$. In both cases we have used $\omega = 1$, $t_b = 0.5$, and $W = 8$.

be noted that during the time evolution the system evolves through highly excited states, while the concept of a polaron with a large effective mass is a ground state phenomenon. Emission and subsequent reabsorption of phonons represents the main mechanism for delocalization of the particle in a random potential. For comparison we also include the result for $\lambda = 0$ that shows Anderson's localization.

APPENDIX D: FINITE-SIZE SCALING OF THE SURVIVAL PROBABILITY

In Fig. 6 we present finite-size scaling of the survival probability $\mathcal{O}(t)$, as defined in Eq. (5) of the main text, in the

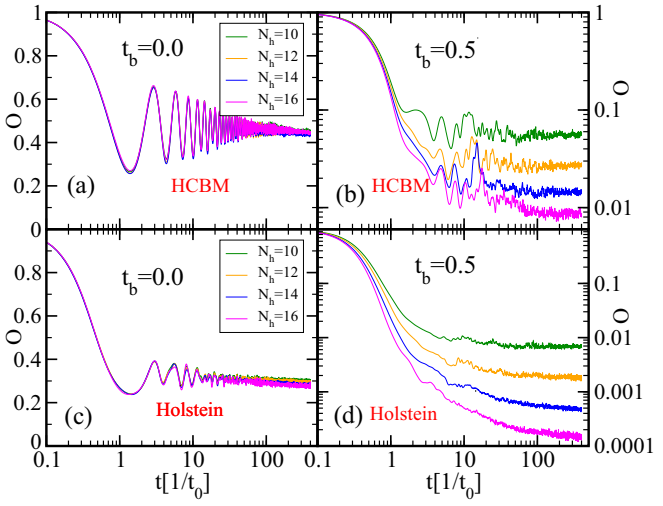

FIG. 6. $\mathcal{O}(t)$ as given in Eq. (5) of the main text using different system sizes as given by N_h, for the HCB model in (a) and (b) and the Holstein model in (b) and (d). In all cases we have used $\omega = g = 1$, $W = 12$.

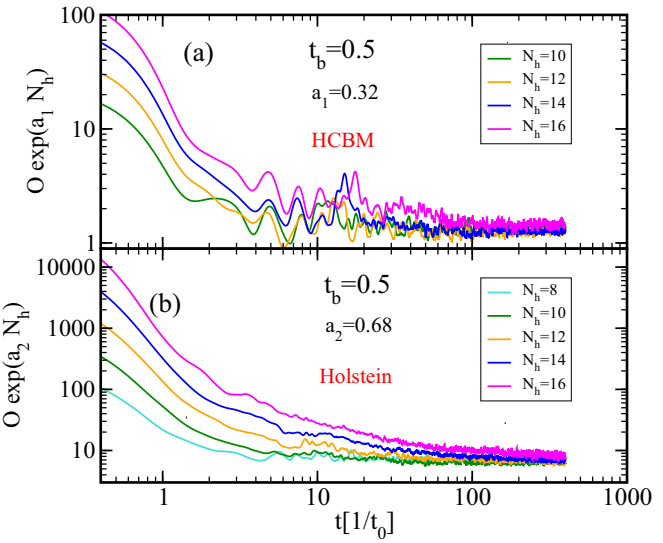

FIG. 7. Scaled survival probability $\mathcal{O}(t)\exp(a_i N_h)$ for the case when $t_b = 0.5$ for the two models as indicated in the figure. In both cases we have used $\omega = g = 1$, $W = 12$.

limit of large disorder, $W = 12$. In the case of localized bosons, i.e., at $t_b = 0$, see Figs. 6(a) and 6(c), we observe near complete overlap of results obtained using system sizes ranging from 10^3 states in cases of $N_h = 10$ through 10^6 in the case of $N_h = 16$. In contrast, in the case of itinerant bosons, for $t_b = 0.5$, we observe a substantial N_h dependence of $\mathcal{O}(t \gg 1)$ in both models; see Figs. 6(b) and 6(d). Note also that in contrast to the previous case, the latter results are presented on a log-log scale. Then, almost equally spaced flat sections of $\mathcal{O}(t \gg 1)$ obtained for $N_h = 10, 12, 14, \ldots$ indicate that the survival probability scales exponentially with the system size L that, in our method, is given by $L \sim N_h$, i.e., $\mathcal{O}(t \gg 1) \propto \exp(-aN_h)$.

In order to obtain a more quantitative picture of the above mentioned exponential scaling we present in Fig. 7 $\mathcal{O}(t)\exp(a_i N_h)$, where $i = 1,2$ for the two models under consideration. A nearly perfect scaling is observed for $t \gg 1$.

It is beneficial to stress two important properties of the localized state in systems with $t_b = 0$. On the one hand, there is an extremely long-time scale which governs the particle dynamics for $t \gtrsim 10^2$, as is clearly visible in Figs. 2(a) and 3(a) in the main text. Such slow dynamics is characteristic for MBL systems [42,70], whereas it does not arise in the Anderson insulators ($g = 0$) where the spreading of particle saturates already at $t \sim 10$. On the other hand, the survival probability does not show any clear exponential decay with the system size, as is the case in the MBL [73]. The survival probability in the studied electron-phonon system with $t_b = 0$ resembles rather the projection of single-particle wave functions $\langle\psi_{sp}(0)|\psi_{sp}(t)\rangle$ in the Anderson insulators, which is, for the particle under consideration at zero electron-phonon coupling, presented in Fig. 3(c) of the main text.

[1] P. W. Anderson, Absence of diffusion in certain random lattices, Phys. Rev. **109**, 1492 (1958).

[2] P. A. Lee and T. V. Ramakrishnan, Disordered electronic systems, Rev. Mod. Phys. **57**, 287 (1985).

[3] L. Fleishman and P. W. Anderson, Interactions and the anderson transition, Phys. Rev. B **21**, 2366 (1980).

[4] D. M. Basko, I. L. Aleiner, and B. L. Altshuler, Metal–insulator transition in a weakly interacting many-electron system with localized single-particle states, Ann. Phys. **321**, 1126 (2006).

[5] V. Oganesyan and D. A. Huse, Localization of interacting fermions at high temperature, Phys. Rev. B **75**, 155111 (2007).

[6] R. Modak and S. Mukerjee, Many-Body Localization in the Presence of a Single-Particle Mobility Edge, Phys. Rev. Lett. **115**, 230401 (2015).

[7] C. Monthus and T. Garel, Many-body localization transition in a lattice model of interacting fermions: Statistics of renormalized hoppings in configuration space, Phys. Rev. B **81**, 134202 (2010).

[8] D. J. Luitz, N. Laflorencie, and F. Alet, Many-body localization edge in the random-field heisenberg chain, Phys. Rev. B **91**, 081103 (2015).

[9] F. Andraschko, T. Enss, and J. Sirker, Purification and Many-Body Localization in Cold Atomic Gases, Phys. Rev. Lett. **113**, 217201 (2014).

[10] P. Ponte, Z. Papić, F. Huveneers, and D. A. Abanin, Many-Body Localization in Periodically Driven Systems, Phys. Rev. Lett. **114**, 140401 (2015).

[11] A. Lazarides, A. Das, and R. Moessner, Fate of Many-Body Localization Under Periodic Driving, Phys. Rev. Lett. **115**, 030402 (2015).

[12] R. Vasseur, S. A. Parameswaran, and J. E. Moore, Quantum revivals and many-body localization, Phys. Rev. B **91**, 140202 (2015).

[13] M. Serbyn, Z. Papić, and D. A. Abanin, Quantum quenches in the many-body localized phase, Phys. Rev. B **90**, 174302 (2014).

[14] D. Pekker, G. Refael, E. Altman, E. Demler, and V. Oganesyan, Hilbert-Glass Transition: New Universality Of Temperature-Tuned Many-Body Dynamical Quantum Criticality, Phys. Rev. X **4**, 011052 (2014).

[15] E. J. Torres-Herrera and L. F. Santos, Dynamics at the many-body localization transition, Phys. Rev. B **92**, 014208 (2015).

[16] M. Távora, E. J. Torres-Herrera, and L. F. Santos, Inevitable power-law behavior of isolated many-body quantum systems and how it anticipates thermalization, Phys. Rev. A **94**, 041603 (2016).

[17] C. R. Laumann, A. Pal, and A. Scardicchio, Many-Body Mobility Edge in a Mean-Field Quantum Spin Glass, Phys. Rev. Lett. **113**, 200405 (2014).

[18] D. A. Huse, R. Nandkishore, and V. Oganesyan, Phenomenology of fully many-body-localized systems, Phys. Rev. B **90**, 174202 (2014).

[19] S. Gopalakrishnan, K. R. Islam, and M. Knap, Noise-Induced Subdiffusion in Strongly Localized Quantum Systems, Phys. Rev. Lett. **119**, 046601 (2017).

[20] J. Hauschild, F. Heidrich-Meisner, and F. Pollmann, Domain-wall melting as a probe of many-body localization, Phys. Rev. B **94**, 161109 (2016).

[21] J. Herbrych, J. Kokalj, and P. Prelovšek, Local Spin Relaxation Within the Random Heisenberg Chain, Phys. Rev. Lett. **111**, 147203 (2013).

[22] J. Z. Imbrie, Diagonalization and Many-Body Localization for a Disordered Quantum Spin Chain, Phys. Rev. Lett. **117**, 027201 (2016).

[23] R. Steinigeweg, J. Herbrych, F. Pollmann, and W. Brenig, Typicality approach to the optical conductivity in thermal and many-body localized phases, Phys. Rev. B **94**, 180401 (2016).

[24] S. S. Kondov, W. R. McGehee, W. Xu, and B. DeMarco, Disorder-Induced Localization in a Strongly Correlated Atomic Hubbard Gas, Phys. Rev. Lett. **114**, 083002 (2015).

[25] M. Schreiber, S. S. Hodgman, P. Bordia, H. P. Lüschen, M. H. Fischer, R. Vosk, E. Altman, U. Schneider, and I. Bloch, Observation of many-body localization of interacting fermions in a quasi-random optical lattice, Science **349**, 842 (2015).

[26] J.-Y. Choi, S. Hild, J. Zeiher, P. Schauß, A. Rubio-Abadal, T. Yefsah, V. Khemani, D. A. Huse, I. Bloch, and C. Gross, Exploring the many-body localization transition in two dimensions, Science **352**, 1547 (2016).

[27] P. Bordia, H. P. Lüschen, S. S. Hodgman, M. Schreiber, I. Bloch, and U. Schneider, Coupling Identical 1D Many-Body Localized Systems, Phys. Rev. Lett. **116**, 140401 (2016).

[28] P. Bordia, H. Lüschen, S. Scherg, S. Gopalakrishnan, M. Knap, U. Schneider, and I. Bloch, Probing Slow Relaxation and Many-Body Localization in Two-Dimensional Quasiperiodic Systems, Phys. Rev. X **7**, 041047 (2017).

[29] J. Smith, A. Lee, P. Richerme, B. Neyenhuis, P. W. Hess, P. Hauke, M. Heyl, D. A. Huse, and C. Monroe, Many-body localization in a quantum simulator with programmable random disorder, Nat. Phys. **12**, 907 (2016).

[30] M. Žnidarič, T. Prosen, and P. Prelovšek, Many-body localization in the heisenberg XXZ magnet in a random field, Phys. Rev. B **77**, 064426 (2008).

[31] J. H. Bardarson, F. Pollmann, and J. E. Moore, Unbounded Growth of Entanglement in Models of Many-Body Localization, Phys. Rev. Lett. **109**, 017202 (2012).

[32] J. A. Kjäll, J. H. Bardarson, and F. Pollmann, Many-Body Localization in a Disordered Quantum Ising Chain, Phys. Rev. Lett. **113**, 107204 (2014).

[33] M. Serbyn, Z. Papić, and D. A. Abanin, Criterion for Many-Body Localization-Delocalization Phase Transition, Phys. Rev. X **5**, 041047 (2015).

[34] D. J. Luitz, N. Laflorencie, and F. Alet, Extended slow dynamical regime prefiguring the many-body localization transition, Phys. Rev. B **93**, 060201 (2016).

[35] M. Serbyn, Z. Papić, and D. A. Abanin, Universal Slow Growth of Entanglement in Interacting Strongly Disordered Systems, Phys. Rev. Lett. **110**, 260601 (2013).

[36] S. Bera, H. Schomerus, F. Heidrich-Meisner, and J. H. Bardarson, Many-Body Localization Characterized from a One-Particle Perspective, Phys. Rev. Lett. **115**, 046603 (2015).

[37] E. Altman and R. Vosk, Universal dynamics and renormalization in many-body-localized systems, Annu. Rev. Condens. Matter Phys. **6**, 383 (2015).

[38] K. Agarwal, S. Gopalakrishnan, M. Knap, M. Müller, and E. Demler, Anomalous Diffusion and Griffiths Effects Near the Many-Body Localization Transition, Phys. Rev. Lett. **114**, 160401 (2015).

[39] S. Gopalakrishnan, M. Müller, V. Khemani, M. Knap, E. Demler, and D. A. Huse, Low-frequency conductivity in many-body localized systems, Phys. Rev. B **92**, 104202 (2015).
[40] M. Žnidarič, A. Scardicchio, and V. K. Varma, Diffusive and Subdiffusive Spin Transport in the Ergodic Phase of a Many-Body Localizable System, Phys. Rev. Lett. **117**, 040601 (2016).
[41] H. P. Lüschen, P. Bordia, S. Scherg, F. Alet, E. Altman, U. Schneider, and I. Bloch, Observation of Slow Dynamics near the Many-Body Localization Transition in One-Dimensional Quasiperiodic Systems, Phys. Rev. Lett. **119**, 260401 (2017).
[42] M. Mierzejewski, J. Herbrych, and P. Prelovšek, Universal dynamics of density correlations at the transition to the many-body localized state, Phys. Rev. B **94**, 224207 (2016).
[43] M. Kozarzewski, P. Prelovšek, and M. Mierzejewski, Distinctive response of many-body localized systems to a strong electric field, Phys. Rev. B **93**, 235151 (2016).
[44] Y. Bar Lev and D. R. Reichman, Dynamics of many-body localization, Phys. Rev. B **89**, 220201 (2014).
[45] Y. Bar Lev, G. Cohen, and D. R. Reichman, Absence of Diffusion in an Interacting System of Spinless Fermions on a One-Dimensional Disordered Lattice, Phys. Rev. Lett. **114**, 100601 (2015).
[46] O. S. Barišić, J. Kokalj, I. Balog, and P. Prelovšek, Dynamical conductivity and its fluctuations along the crossover to many-body localization, Phys. Rev. B **94**, 045126 (2016).
[47] J. Bonča and M. Mierzejewski, Delocalized carriers in the t-j model with strong charge disorder, Phys. Rev. B **95**, 214201 (2017).
[48] P. Sierant, D. Delande, and J. Zakrzewski, Many-body localization due to random interactions, Phys. Rev. A **95**, 021601 (2017).
[49] N. F. Mott, Conduction in glasses containing transition metal ions, J. Non-Cryst. Solids **1**, 1 (1968).
[50] D. Emin, Phonon-assisted transition rates I. Optical-phonon-assisted hopping in solids, Adv. Phys. **24**, 305 (1975).
[51] D. Di Sante, S. Fratini, V. Dobrosavljević, and S. Ciuchi, Disorder-Driven Metal-Insulator Transitions in Deformable Lattices, Phys. Rev. Lett. **118**, 036602 (2017).
[52] Y. Yao, Polaronic quantum diffusion in dynamic localization regime, New J. Phys. **19**, 043015 (2017).
[53] S. A. Parameswaran and S. Gopalakrishnan, Spin-catalyzed hopping conductivity in disordered strongly interacting quantum wires, Phys. Rev. B **95**, 024201 (2017).
[54] P. Prelovšek, O. S. Barišić, and M. Žnidarič, Absence of full many-body localization in the disordered Hubbard chain, Phys. Rev. B **94**, 241104 (2016).
[55] A. Chandran, V. Khemani, C. R. Laumann, and S. L. Sondhi, Many-body localization and symmetry-protected topological order, Phys. Rev. B **89**, 144201 (2014).
[56] A. C. Potter and R. Vasseur, Symmetry constraints on many-body localization, Phys. Rev. B **94**, 224206 (2016).
[57] I. V. Protopopov, W. W. Ho, and D. A. Abanin, Effect of SU(2) symmetry on many-body localization and thermalization, Phys. Rev. B **96**, 041122 (2017).
[58] R. Mondaini and M. Rigol, Many-body localization and thermalization in disordered hubbard chains, Phys. Rev. A **92**, 041601(R) (2015).
[59] J. Bonca, S. A. Trugman, and I. Batistić, Holstein polaron, Phys. Rev. B **60**, 1633 (1999).
[60] S. Dal Conte, L. Vidmar, D. Golez, M. Mierzejewski, G. Soavi, S. Peli, F. Banfi, G. Ferrini, R. Comin, B. M. Ludbrook, L. Chauviere, N. D. Zhigadlo, H. Eisaki, M. Greven, S. Lupi, A. Damascelli, D. Brida, M. Capone, J. Bonca, G. Cerullo, and C. Giannetti, Snapshots of the retarded interaction of charge carriers with ultrafast fluctuations in cuprates, Nat. Phys. **11**, 421 (2015).
[61] D. Golež, J. Bonča, M. Mierzejewski, and L. Vidmar, Mechanism of ultrafast relaxation of a photo-carrier in antiferromagnetic spin background, Phys. Rev. B **89**, 165118 (2014).
[62] M. Mierzejewski, L. Vidmar, J. Bonča, and P. Prelovšek, Nonequilibrium Quantum Dynamics of a Charge Carrier Doped into a Mott Insulator, Phys. Rev. Lett. **106**, 196401 (2011).
[63] J. Bonča, S. Maekawa, and T. Tohyama, Numerical approach to the low-doping regime of the t–J model, Phys. Rev. B **76**, 035121 (2007).
[64] D. Golež, J. Bonča, L. Vidmar, and S. A. Trugman, Relaxation Dynamics of the Holstein Polaron, Phys. Rev. Lett. **109**, 236402 (2012).
[65] L. Vidmar, J. Bonča, M. Mierzejewski, P. Prelovšek, and S. A. Trugman, Nonequilibrium dynamics of the holstein polaron driven by an external electric field, Phys. Rev. B **83**, 134301 (2011).
[66] J. Kogoj, L. Vidmar, M. Mierzejewski, S. A. Trugman, and J. Bonča, Thermalization after photoexcitation from the perspective of optical spectroscopy, Phys. Rev. B **94**, 014304 (2016).
[67] J. Kogoj, M. Mierzejewski, and J. Bonča, Nature of Bosonic Excitations Revealed by High-Energy Charge Carriers, Phys. Rev. Lett. **117**, 227002 (2016).
[68] D. Schmidtke, R. Steinigeweg, J. Herbrych, and J. Gemmer, Interaction-induced weakening of localization in few-particle disordered heisenberg chains, Phys. Rev. B **95**, 134201 (2017).
[69] N. F. Mott, Conduction in non-crystalline materials, Philos. Mag. **19**, 835 (1969).
[70] P. Prelovšek, M. Mierzejewski, O. Barišić, and J. Herbrych, Density correlations and transport in models of many-body localization, Ann. Phys. **529**, 1600362 (2017).
[71] S. Banerjee and E. Altman, Variable-Range Hopping through Marginally Localized Phonons, Phys. Rev. Lett. **116**, 116601 (2016).
[72] M. Heyl, Dynamical Quantum Phase Transitions in Systems with Broken-Symmetry Phases, Phys. Rev. Lett. **113**, 205701 (2014).
[73] P. Prelovšek, O. S. Barišić, and M. Mierzejewski, Reduced-basis approach to many-body localization, Phys. Rev. B **97**, 035104 (2018).
[74] D. Golež, J. Bonča, and L. Vidmar, Dissociation of a hubbard-holstein bipolaron driven away from equilibrium by a constant electric field, Phys. Rev. B **85**, 144304 (2012).